AGU PUBLICATIONS

JGR

Journal of Geophysical Research: Oceans

RESEARCH ARTICLE

10.1002/2013JC009528

Key Points:
- The centrifugal force is important in Mozambique Channel rings
- We propose to include inertia when deriving currents from sea surface height
- Inclusion of inertia results in a net improvement when computing ocean currents

Correspondence to:
P. Penven,
pierrick.penven@ird.fr

Citation:
Penven, P., I. Halo, S. Pous, and L. Marié (2014), Cyclogeostrophic balance in the Mozambique Channel, *J. Geophys. Res. Oceans*, *119*, doi:10.1002/2013JC009528.

Received 22 OCT 2013
Accepted 26 JAN 2014
Accepted article online 31 JAN 2014

Cyclogeostrophic balance in the Mozambique Channel

Pierrick Penven[1,2,3], Issufo Halo[2,4], Stéphane Pous[2,3,5], and Louis Marié[1]

[1]Laboratoire de Physique des Océans, UMR 6523 (CNRS, Ifremer, IRD, UBO), Plouzané, France, [2]Department of Oceanography, University of Cape Town, Cape Town, South Africa, [3]LMI ICEMASA, IRD, University of Cape Town, Cape Town, South Africa, [4]Nansen-Tutu Centre for Marine Environmental Research, University of Cape Town, Cape Town, South Africa, [5]Laboratoire d'Océanographie et du Climat: Expérimentations et Approches Numériques, UMR 7159 (CNRS, IRD, MHN, UPMC), Paris, France

Abstract Three methods are proposed for the inclusion of inertia when deriving currents from sea surface height (SSH) in the Mozambique Channel: gradient wind, perturbation expansion, and an iterative method. They are tested in a model and applied to satellite altimetry. For an eddy of 25 cm amplitude and 100 km radius, typical of Mozambique Channel rings at 18°S, the error made with geostrophy is 40% for the anticyclones and 20% for the cyclones. Inertia could reach one third of the pressure gradient. Geostrophy underestimates subsurface currents by up to 50 cm s^{-1}, resulting in errors of 30–40%. The iterative method results in errors of <5% for the most part of the structure. The error RMS in velocities based on 8 years of model SSH is in excess of 30 cm s^{-1} for geostrophy and reduces to about 10 cm s^{-1} for the gradient wind and iterative methods. The perturbation method is less accurate. Applied to satellite altimetry, the addition of inertia results in a significant increase in velocities for the anticyclones and a decrease for the cyclones. It induces a velocity increase of >50% in Mozambique Channel rings. Geostrophic EKE reaches 1400 cm^2 s^{-2}, while it attains 1800 cm^2 s^{-2} when inertia is added. Applied to the Gulf Stream, these methods confirm the hypothesis of *Maximenko and Niiler* [2006] that centrifugal accelerations should be the main cause for the difference observed between geostrophic and drifter EKE. This methodology should result in a net improvement for operational surface ocean currents.

1. Introduction

The Mozambique Channel is located at the western side of the Indian Ocean, between the African Continent and Madagascar (Figure 1a). The oceanic circulation is here highly energetic, principally in the form of large Mozambique Channel rings propagating through the Channel (Figure 1a) [*Halo et al*., 2014]. Satellite altimetry has been extensively used to follow Mozambique Channel rings and eddies [*Backeberg et al*., 2012; *de Ruijter et al*., 2002, 2004; *Gründlingh*, 1995; *Halo et al*., 2014; *Quartly and Srokosz*, 2003; *Schouten et al*., 2003; *Swart et al*., 2010; *Ternon et al*., 2014; *Tew-Kai et al*., 2009; *Weimerskirch et al*., 2004]. The derivation of ocean currents and eddies from gridded satellite altimetry [*Ducet et al*., 2000] is in general based on the hypothesis of the existence of an equilibrium between the Coriolis force and the pressure gradient, the geostrophic balance:

$$f\boldsymbol{k}\times\boldsymbol{u_g}=-g\nabla\eta, \tag{1}$$

where f is the Coriolis parameter, $\boldsymbol{k}$ is the vertical unit vector, $\boldsymbol{u_g}$ is the geostrophic velocity vector, and η is the sea surface height (SSH). Second derivatives of (1) are often used at the Equator [*Picaut et al*., 1989] and an Ekman regression model could also be added to account for the wind effects [*Lagerloef et al*., 1999].

In the Mozambique Channel, a recent comparison between altimetric geostrophic currents and in situ observations has shown large differences: "During both cruises the altimetry observations underestimated the velocities observed from the ADCP measurements by about 30% (...) geostrophic current derived from altimetry indicates that the geostrophic velocities are some 21% lower than those of the drifters" [*Ternon et al*., 2014]. This shows a possible limitation when using the geostrophic balance in the Mozambique Channel.

Rings and eddies in the Mozambique Channel have been recently analyzed from models and altimetry by *Halo et al*. [2014]. They have shown that the mean eddy amplitude per class of eddy radius is in general

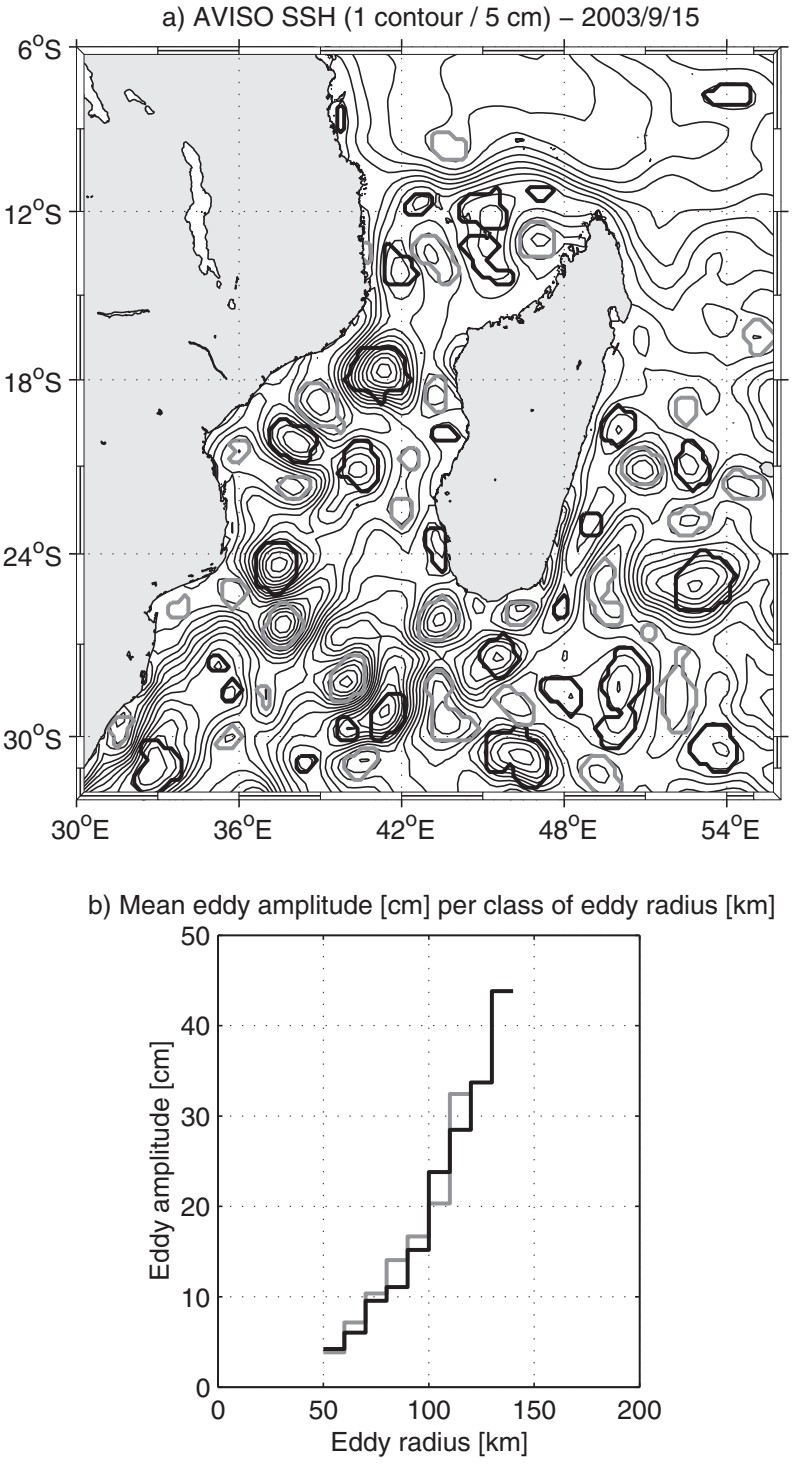

Figure 1. (a) Gridded absolute dynamic topography observed over the Mozambique Channel for the 15 September 2003 (the date used by *Weimerskirch et al.* [2004]). The eddies detected using the method described by *Halo et al.* [2014] are highlighted in black lines for the anticyclones and in gray lines for the cyclones. (b) Mean eddy amplitude per class of eddy radius from the eddies detected based on AVISO altimetry from 14 October 1992 to 31 March 2010. The black lines represent the anticyclones and the gray lines the cyclones. Figure adapted from *Halo et al.* [2014].

larger for the cyclones than for the anticyclones (Figure 1b). *Halo et al.* [2014] have hypothesized that this asymmetry could be caused by the centrifugal acceleration. This acceleration being always directed outward, for a given eddy velocity, a larger pressure gradient (i.e., a larger amplitude in SSH) is necessary to close the balance for a cyclone than for an anticyclone [*Maximenko and Niiler*, 2006].

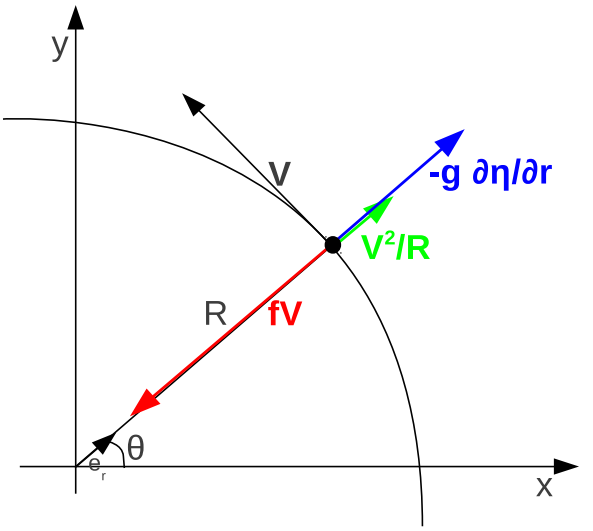

Figure 2. Forces in presence in the context of a cyclogeostrophic balance for an anticyclonic eddy in the Southern Hemisphere.

It is known that in regions of western boundary currents the advection of momentum is in general not negligible [*Charney*, 1955] and, if this is the case, centrifugal accelerations could be significant in mesoscale vortices and meanders [*Bakun*, 2006]. For a given horizontal pressure field, the neglect of centrifugal accelerations would result in an overestimation of the velocities in the cyclonic eddies and an underestimation in the anticyclonic eddies [*Maximenko and Niiler*, 2006]. This bias has been hypothesized (albeit without direct quantification) by *Maximenko and Niiler* [2006] as a possible explanation for the systematic difference in eddy kinetic energy (EKE) derived from surface drifters and from geostrophic currents obtained from altimetry seen in the Gulf Stream region [*Fratantoni*, 2001].

Here we propose that centrifugal accelerations, and in general inertial effects, are of importance for the surface ocean dynamics in the Mozambique Channel. The gradient wind equation, known for a long time in atmospheric science [*Gold*, 1908; *Holton*, 1992; *Knox and Ohmann*, 2006], allows the derivation of horizontal wind velocities from a pressure field in presence of centrifugal accelerations. This equation has been widely used in atmospheric science, and can predict a wind field from a given pressure field with an accuracy of 5–10% [*Endlich*, 1961]. In the present work, the gradient wind equation is adapted for the use with altimetry SSH in the ocean and is tested in a realistic numerical simulation of the eddies in the Mozambique Channel.

2. Material and Methods

2.1. The SSH Inversion Problem

In the context of an horizontal, stationary, and inviscid flow, the momentum equation which links SSH and surface horizontal currents $\boldsymbol{u}$ is

$$\boldsymbol{u}.\nabla\boldsymbol{u}+f\boldsymbol{k}\times\boldsymbol{u}=-g\nabla\eta. \tag{2}$$

Introducing the geostrophic velocities $\boldsymbol{u_g}$ from (1), this equation can be transformed to the form

$$\boldsymbol{u}-\frac{\boldsymbol{k}}{f}\times(\boldsymbol{u}.\nabla\boldsymbol{u})=\boldsymbol{u_g}. \tag{3}$$

As stated by *Arnason et al.* [1962], solving this equation in full generality is a difficult task. Approximate solutions can however be derived in a variety of contexts, of which we will now discuss a few.

2.2. Cyclogeostrophic/Gradient Wind Equation

In axisymmetric cases, the $\boldsymbol{u}.\nabla\boldsymbol{u}$ nonlinear term simplifies to the centrifugal acceleration term $-\frac{V^2}{R}\boldsymbol{e_r}$, with V the azimuthal component of velocity, R the radius of curvature, and $\boldsymbol{e_r}$ the outward-directed radial unit vector (see Figure 2). In this case, (3) simplifies for the azimuthal velocities to the gradient wind equation [*Gold*, 1908; *Holton*, 1992; *Knox and Ohmann*, 2006]:

$$V+\frac{V^2}{fR}=V_g, \tag{4}$$

where V_g is the geostrophic velocity. This equation can be solved analytically for V, with result:

$$V=\frac{2V_g}{1\pm\sqrt{1+4V_g/(fR)}}. \tag{5}$$

The "normal" solution corresponds to the positive sign. In the context of an anticyclonic eddy of small radius R ($V_g>0$ in the southern hemisphere, see Figure 2), the term inside the square root can be negative, resulting in the absence of a physical solution for (4). This is in general associated with the occurrence of inertial instability [*Knox and Ohmann*, 2006]. In this case, other terms (such as viscosity or tendency) should gain importance in the momentum balance.

The gradient wind solution can be extended by applying point-wise the approximate solution (5), using local estimates of the curvature radius R of the trajectories of fluid particles, assumed to flow along iso-SSH curves. Since the centrifugal force is perpendicular to the fluid particles trajectories, and hence is parallel to the Coriolis force (see Figure 2), the gradient wind velocities are parallel to the geostrophic velocities. Expressing $\boldsymbol{u}$ as $V\boldsymbol{t}$, with $\boldsymbol{t}$ the unit vector tangent to the local iso-SSH curve, one can express the local curvature radius of the trajectories as $R=1/|\boldsymbol{\kappa}|$, with κ the curvature vector defined as $\boldsymbol{\kappa}=(\boldsymbol{t}.\nabla)\boldsymbol{t}$ [*Callen*, 2003].

2.3. Perturbation Expansion

Nondimensionalizing respectively horizontal distances and velocities by the scales L and U in (3) and introducing the Rossby number $\varepsilon=\frac{U}{fL}$, gives:

$$\boldsymbol{u}-\varepsilon\boldsymbol{k}\times(\boldsymbol{u}.\nabla\boldsymbol{u})=\boldsymbol{u_g}. \tag{6}$$

An expansion in powers of ε is introduced for the surface current vector $\boldsymbol{u}$. The solution of (6) to order 0 in ε is the geostrophic approximation. Carrying the calculation one more order provides a refined solution $\boldsymbol{u}_{\mathrm{per}}$ as:

$$\boldsymbol{u_{per}}=\boldsymbol{u_g}+\varepsilon\boldsymbol{k}\times(\boldsymbol{u_g}.\nabla\boldsymbol{u_g}). \tag{7}$$

Higher-order solutions could also be obtained by reinjecting this solution in (6). Dimensionally, solution (7) resumes to:

$$\boldsymbol{u_{per}}=\boldsymbol{u_g}+\frac{\boldsymbol{k}}{f}\times(\boldsymbol{u_g}.\nabla\boldsymbol{u_g}). \tag{8}$$

2.4. Iterative Method

In atmospheric science, *Arnason et al.* [1962] and *Endlich* [1961] have proposed approximate solutions of the gradient wind equation based on iterative methods. For (3), they proposed an iterative scheme of the form:

$$\boldsymbol{u}^{(n+1)}=\boldsymbol{u_g}+\frac{\boldsymbol{k}}{f}\times(\boldsymbol{u}^{(n)}.\nabla\boldsymbol{u}^{(n)}). \tag{9}$$

This scheme is known to diverge under certain conditions [*Arnason et al.*, 1962], especially where (4) does not hold a solution. Consequently, we have decided to iterate point by point (9) until the residual $res=|\boldsymbol{u}^{(n+1)}-\boldsymbol{u}^{(n)}|$ is below $res=0.01$ m s^{-1} or start to increase.

2.5. SWIM Ocean Model Simulation and AVISO SSH

The methods detailed in sections 2.2, 2.3, and 2.4 are evaluated against the outputs of a regional model of the Mozambique Channel: SWIM (South West Indian ocean Model) [*Halo*, 2012; *Halo et al.*, 2014]. SWIM has

been specifically designed for the explicit resolution of the highly energetic Mozambique Channel rings and eddies [*Halo*, 2012; *Halo et al*., 2014]. It simulates the ocean dynamics in the Mozambique Channel with a horizontal grid resolution of approximately 20 km [*Halo*, 2012]. The ability of SWIM to accurately reproduce the mean dynamics, mean hydrography, the seasonal cycle and the eddy variability of the South-West Indian Ocean has been demonstrated by *Halo* [2012] and *Halo et al*. [2014]. To derive the momentum balance in a typical Mozambique Channel ring, SWIM has been rerun for the month of February of model year 2010, storing all the terms of the momentum equation with a 2 days averaged sampling.

Observed SSH is based on the homogeneous gridded absolute dynamic topography data obtained from AVISO [*Ducet et al*., 2000]. Absolute dynamic topography is derived by combining measured sea level anomaly data from satellites with the *Rio et al*. [2011] mean dynamic topography.

3. Results

3.1. Analytical Evaluation of the Methods in an Axisymmetric Gaussian Eddy

Solutions (5) and (7) are compared to the geostrophic currents in the case of an axisymmetric Gaussian eddy of the form $\eta=\eta_0 \exp -(r/R_0)^2$ in the southern hemisphere. In this case, the geostrophic azimuthal velocity V_g is

$$V_g=-\frac{g\eta_0}{fR_0}\frac{r}{R_0}\exp -(r/R_0)^2,$$

the gradient wind azimuthal velocity V_{gr} is

$$V_{gr}=\frac{2V_g}{1+\sqrt{1+4V_g/(fr)}},$$

and the perturbation expansion results in

$$V_{per}=V_g-\frac{V_g^2}{fr}.$$

Figure 3 displays the eddy azimuthal velocities for several eddy e-folding scales R_0 (from 50 to 250 km) and eddy amplitudes η_0 ($\pm$25 and $\pm$50 cm). For R_0 larger than 200 km and for the 4 values of η_0, we are in a valid regime of geostrophic balance with errors $<$15%.

Inertial effects start to be significant below this scale. For 100 km $< R_0 <$ 200 km, the gradient wind and perturbation solutions are relatively close to each other, but clearly depart from geostrophy. Figure 3 complies with the argument of *Maximenko and Niiler* [2006] that geostrophy exaggerates velocities in cyclones and underestimates them in anticyclones. For a SSH anomaly of 25 cm and an eddy radius of 100 km (which is not uncommon in the Mozambique Channel [*Halo et al*., 2014]), the error made by using geostrophic velocities is $>$40% for the anticyclones and 20% for the cyclones. For $\eta_0 = 50$ cm, the gradient wind equation does not hold a solution for $r <$ 80 km and $R_0 = 100$ km.

For R_0 smaller than 100 km, there are large differences between the gradient wind and the perturbation solutions for the 4 values of η_0. The first-order perturbation approximation made in section 2.3 is no more valid. For $R_0 = 50$ km and $\eta_0 = -50$ cm, the perturbation method results even in anticyclonic velocities close to the center of the cyclone (Figure 3c). For $R_0 = 50$ km and $\eta_0 = 50$ and 25 cm, the gradient wind equation does not have a solution for $r <$ 70 and 58 km, respectively. Note that in the Mozambique Channel, the mean eddy amplitudes vary quasi-linearly from $<$5 cm for an eddy radius of 50 km to about 20 cm for an eddy radius of 100 km (Figure 1b) [*Halo et al*., 2014]. The radical regime of large amplitudes and small diameters seen in Figures 3a and 3c is not a common feature seen from altimetry in the Mozambique Channel.

3.2. Momentum Balance in a Typical Mozambique Channel Ring in SWIM

The derivations made in sections 2.2, 2.3, and 2.4. are tested against the solution of the ocean model SWIM. The model time index has been chosen in order to obtain an eddy with similar characteristics and location

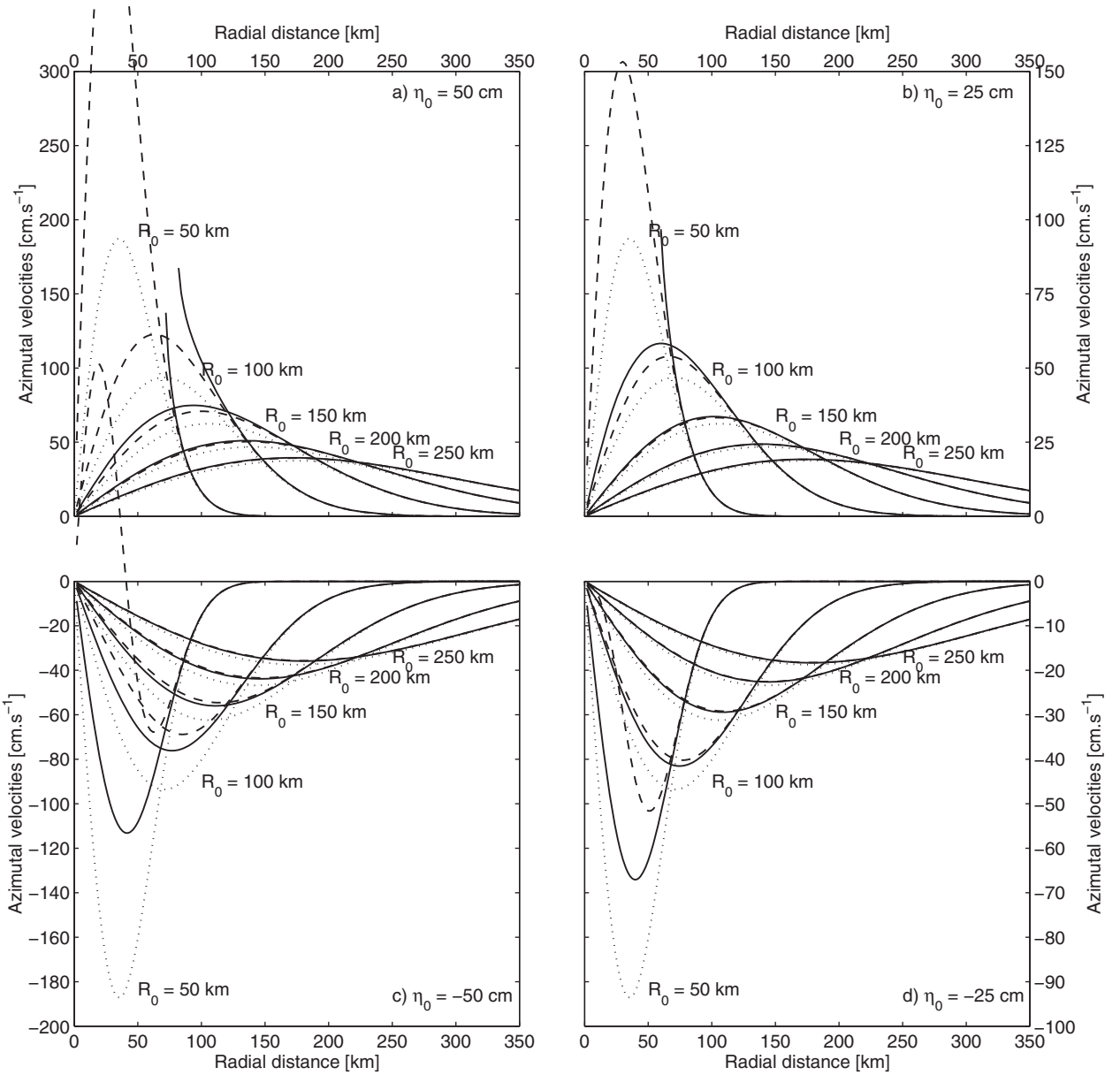

Figure 3. Azimuthal velocities (cm s^{-1}) for an axisymmetric Gaussian eddy of the form $\eta = \eta_0 \exp -(r/R_0)^2$ in the Southern Hemisphere. Plain lines: analytical solutions of the gradient wind equation. Dashed lines: solutions of the perturbation method. Dotted lines: geostrophic velocities. The velocities are represented for several eddy e-folding scales R_0 and for 4 eddy amplitudes η_0: (a) 50 cm, (b) 25 cm, (c) −50 cm, and (d) −25 cm.

as the large anticyclonic ring seen at 18°S in Figure 1a. This location lies exactly in the track of the Mozambique Channel rings detailed by *Halo et al*. [2014]. Figure 4 shows the tendency terms for the first level of the model in the center of the Mozambique Channel for the 6 February of model year 2010. The modeled ring has an amplitude of 40 cm, a radius of 140 km and is located at 40°E longitude and 18.7°S latitude. The model momentum balance shows a dominance of the pressure gradient directed outward and the Coriolis acceleration directed inward (Figure 4a). The advection of momentum is directed outward almost parallel to the pressure gradient. The magnitude is in general not negligible and could reach one third of the pressure gradient. In the northern part of the structure, the ring is not perfectly circular, resulting in a loss of parallelism between the advection of momentum and the pressure gradient. Note that all the other terms (horizontal and vertical mixing, temporal tendency) are also represented but are almost invisible here.

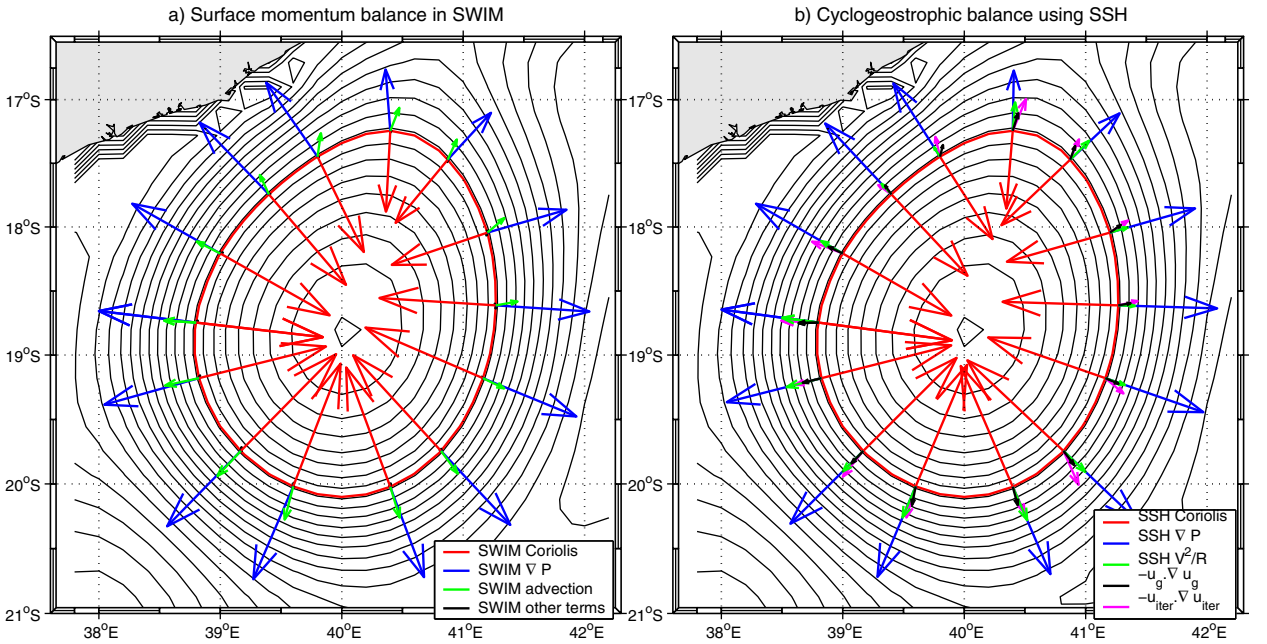

Figure 4. SSH (1 contour/5 cm) of the ocean model SWIM for the 6 February of model year 2010 for a typical Mozambique Channel ring. The SSH is maximum in the center of the ring. (a) The arrows represent the balance of forces in the first model level, acting on a water particle along a selected SSH isoline around the ring. (b) The arrows represent the forces obtained using the gradient wind equation (4) from the model SSH. The momentum advection force obtained from the perturbation method is added as black arrows. The momentum advection force obtained from the iterative method is added in purple.

Figure 4b represents the pressure gradient, the Coriolis acceleration and the centrifugal acceleration calculated from the model SSH using the different methods. In this simplified setting, the balance of dominant terms is almost identical to the one resulting from the complete primitive equations. By construction (see Figure 2), the centrifugal acceleration computed with the gradient wind equation is parallel to the pressure gradient and Coriolis acceleration (green arrows in Figure 4b). The loss of parallelism associated with accelerations/decelerations along the SSH isolines cannot be accounted by this formalism. On the other side, the perturbation method (black arrows in Figure 4b) is able to reflect this process, but underestimates the inertial acceleration by almost a factor of 2. The best approximation in terms of amplitude and direction appears to be obtained by the iterative method (purple arrows in Figure 4b).

3.3. Errors in Computing the Velocities in a Typical Mozambique Channel Ring

SWIM SSH and velocities are used to quantify the error made in computing velocities based on the different methods in this typical Mozambique Channel ring. Figure 5 compares the currents derived from geostrophy, gradient wind, perturbation, and iterative methods with the SWIM velocities at 5 m depth (chosen to limit the effects of the wind). We are here in presence of a highly energetic structure with velocities reaching 2 m s^{-1} (Figure 5b). For this large anticyclone, geostrophic velocities underestimate subsurface currents by up to 50 cm s^{-1} (Figure 5c), resulting in relative errors of the order of 30–40%. These are consistent with the findings of *Ternon et al.* [2014].

The gradient wind method reduces the error to 10 cm s^{-1} or less for the major part of the ring (Figure 5d), the relative errors being of the order of 5–10%, in agreement with *Endlich* [1961]. In the northern side of the ring, where advection is not aligned with pressure gradient and Coriolis acceleration, errors are larger: O (20 cm s^{-1}). They are also large close to the shore, where interaction with coastline and topography could locally lead to other equilibria. More critically, the gradient wind second-order polynomial does not bear a solution in the northern part of the ring, where the curvature is tighter.

As shown in Figure 4b, the perturbation method is able to catch the effects of accelerations/decelerations along the streamlines and accepts a solution in any case. Nevertheless, it still underestimate the velocities by 10–15% for most part of the ring (Figure 5e). This bias is reduced by the iterative method, resulting in a solution at least equivalent to the gradient wind solution in the context of pure cyclogeostrophy, and

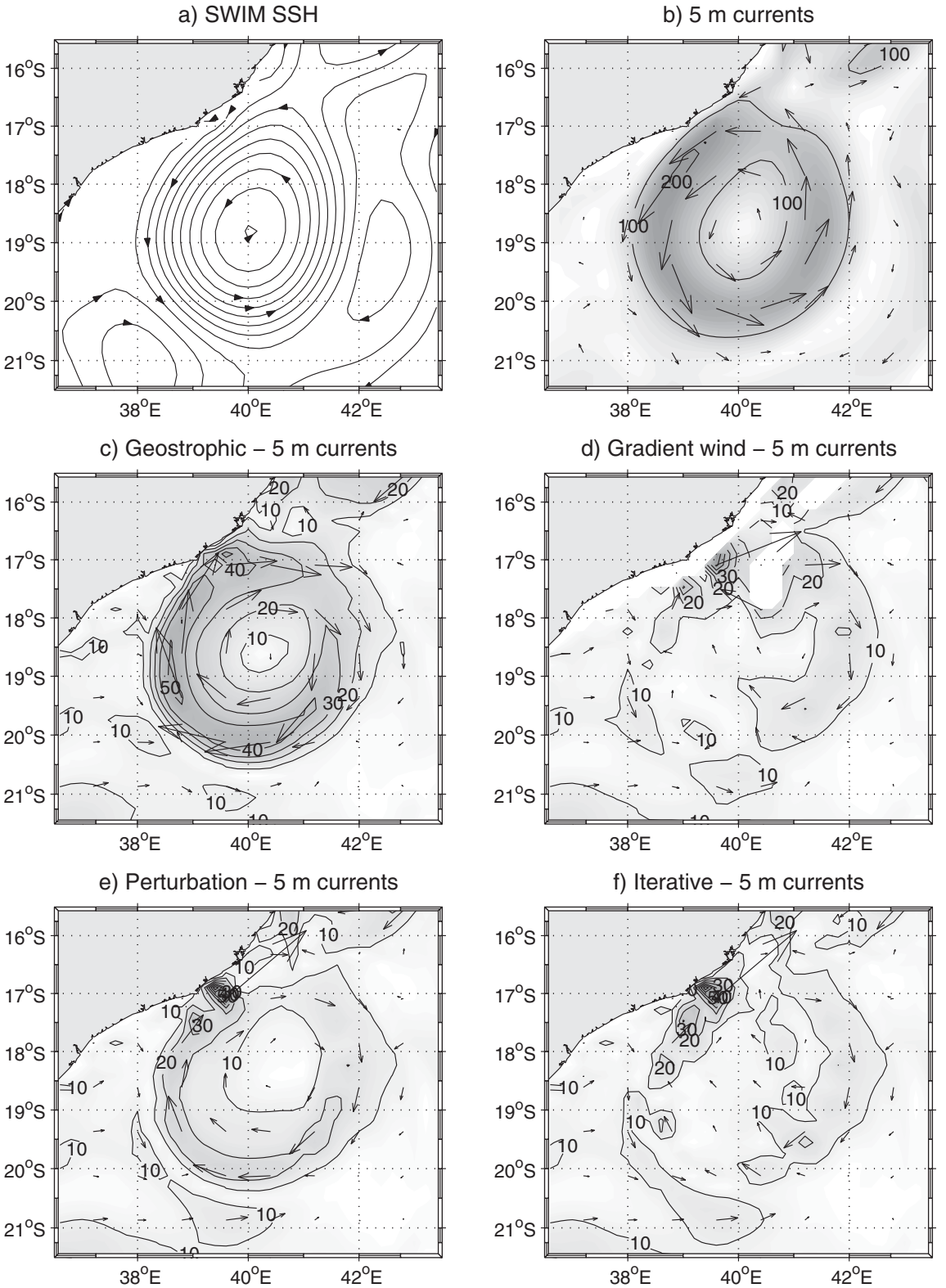

Figure 5. Comparison between model SWIM SSH derived currents and model SWIM subsurface velocities for a typical Mozambique Channel ring for the 6 February of model year 2010. First line: (a) model SSH (1 contour/10 cm) and (b) model velocities at 5 m depth. Second and third lines: (c) difference between SSH-derived velocities and model 5 m velocities for geostrophy, (d) gradient wind (d), (e) the perturbation method, and (f) the iterative method. One vector every four grid points.

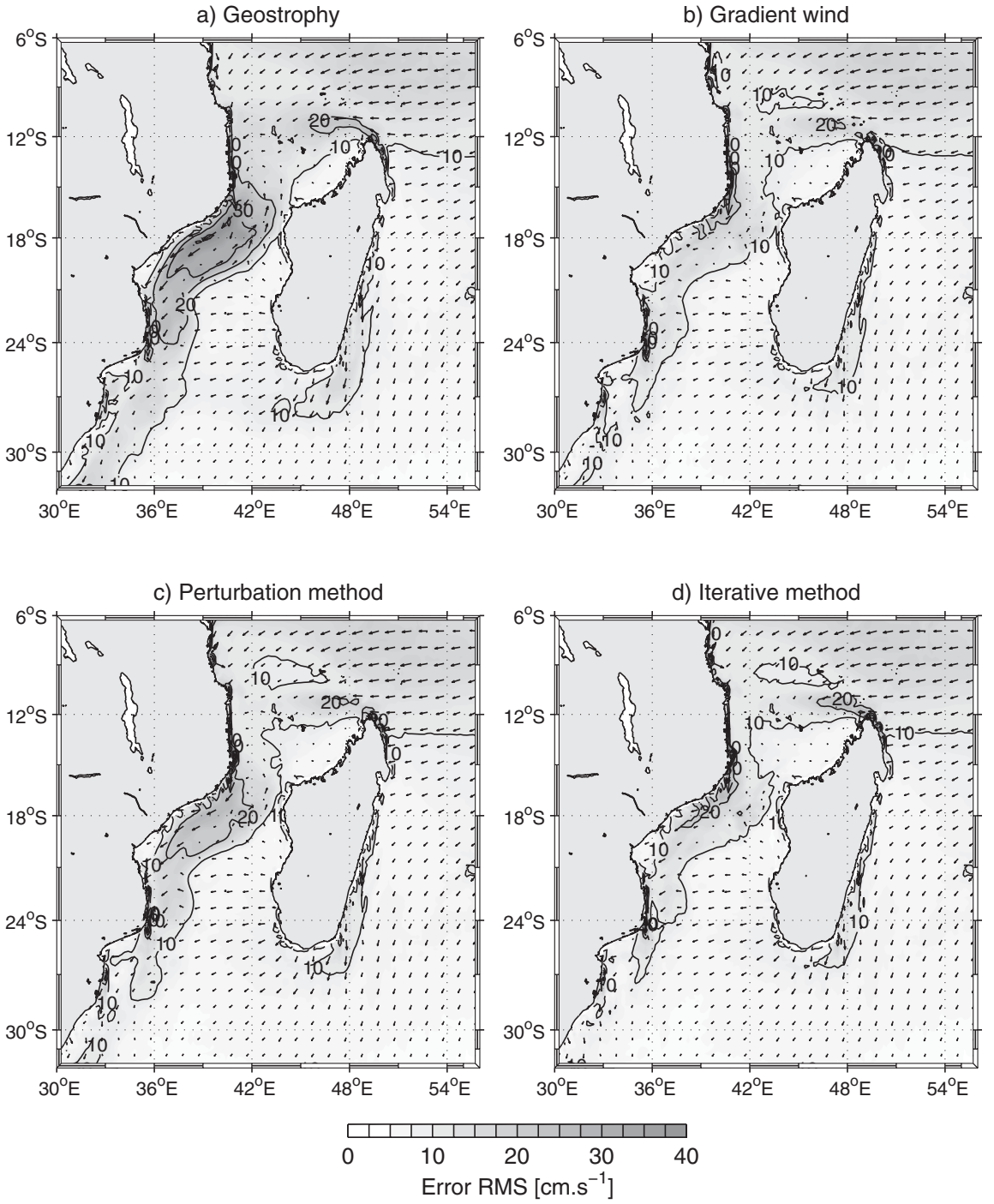

Figure 6. Velocity error RMS (cm s^{-1}) and associated vectors for the velocities derived from SWIM SSH based on 8 years of (a) SWIM simulation using geostrophy, (b) gradient wind, (c) perturbation, and (d) iterative methods. The reference velocities used are the 5 m currents from SWIM. One vector every five grid points.

capturing the accelerations/decelerations processes in the northern side of the ring. It still have difficulties in the immediate vicinity of the shore, but errors are <5% for the majority of the ring (Figure 5f).

3.4. Error RMS in Computing Velocities From SWIM SSH

The evaluation of the different methods can be extended to the full length of the model simulation. Figure 6 presents the error RMS and associated vectors, defined as

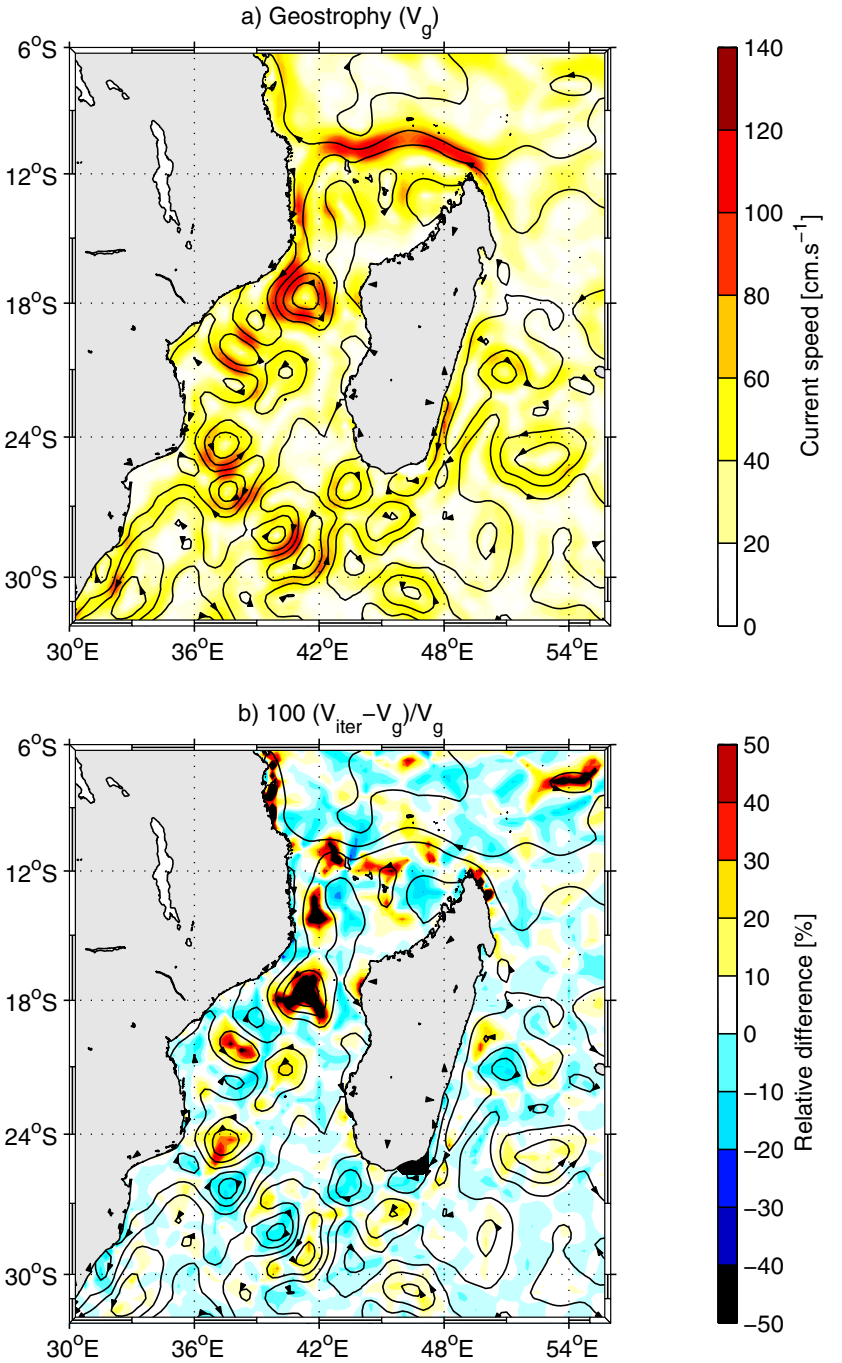

Figure 7. Application of the different methods to satellite altimetry. (a) velocities (cm s^{-1}) derived from satellite SSH for the 15 September 2003 using geostrophy. (b): relative difference (%) of the velocities obtained from the iterative method in regard to geostrophy. Altimetry SSH is added as black contours (1 contour/15 cm).

$$RMS = \sqrt{\frac{\Sigma\left(\left(u_{ref}-u_{app}\right)^2+\left(v_{ref}-v_{app}\right)^2\right)}{N}},$$

where u_{ref} and v_{ref} are SWIM 5 m velocities, u_{app} and v_{app} are the velocities derived from 8 years of SWIM SSH using the different methods, and N the number of model outputs used (here $N = 1440$). For these statistics, we used the solution from the iterative method at the points were no solution existed for the gradient wind second-order polynomial.

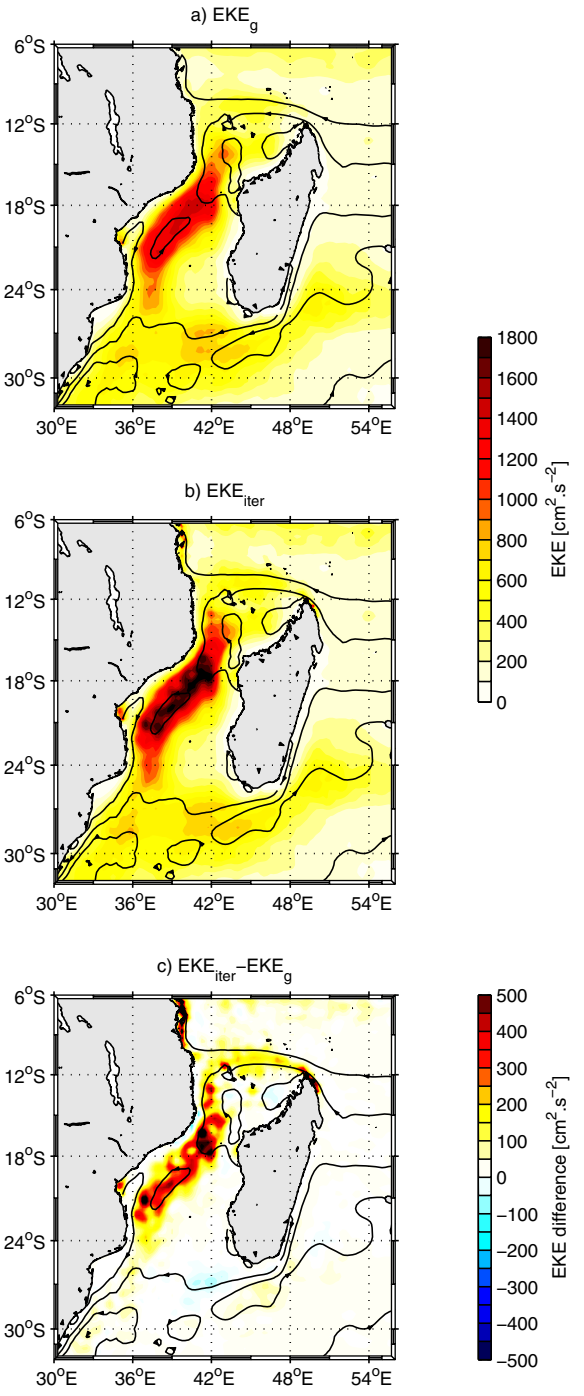

Figure 8. Eddy kinetic energy (EKE) (cm^2 s^{-2}) derived from satellite altimetry using (a) geostrophy and (b) the iterative method. (c) EKE difference (cm^2 s^{-2}) between geostrophy and the iterative method.

As expected, geostrophy results in the largest error RMS, in excess of 30 cm s^{-1} in the central Mozambique Channel (Figure 6a), in the region corresponding to the maximum of eddy kinetic energy (see for example Figure 8a). Errors are also locally large along the inshore edge of the North Madagascar Current where it detaches from the Northern tip of Madagascar. The perturbation method still keep an error in the central Mozambique Channel, but reduced to around 20 cm s^{-1} (Figure 6c). This error diminishes to about 10 cm s^{-1} for the gradient wind and iterative methods (Figures 6b and 6d). The error pattern is equivalent for these two methods, showing significant values of the order of 20 cm s^{-1} locally along the coastlines and in the detachment of the North Madagascar Current. The error is also reduced South of Madagascar and offshore of the Tanzanian coasts. A large-scale background signal, increasing to almost 20 cm s^{-1} toward the Equator is typical of the influence of Ekman currents.

3.5. Application to Satellite Altimetry

An example of the application to derive ocean velocities from altimeter SSH for the 15 September 2003 is given on Figure 7. As argued by *Maximenko and Niiler* [2006], compared to geostrophy, the addition of inertia results in a significant increase in velocities for the anticyclones and a decrease for the cyclones. This effect could reach more than a 50% increase in the large Mozambique Channel rings in the central Mozambique Channel for the gradient wind and iterative methods (Figure 7b). The perturbation method results in a reduced effect (figure not shown). Although the gradient wind and iterative solutions produced equivalent results, the gradient wind second-order polynomial does not held a solution in the center of the large Mozambique Channel ring in the central Mozambique Channel (figure not shown). This is consistent with the homogeneous vorticity structure, typical of the center of the Mozambique Channel rings [*Halo et al*., 2014], hypothesized to be associated with inertial instability.

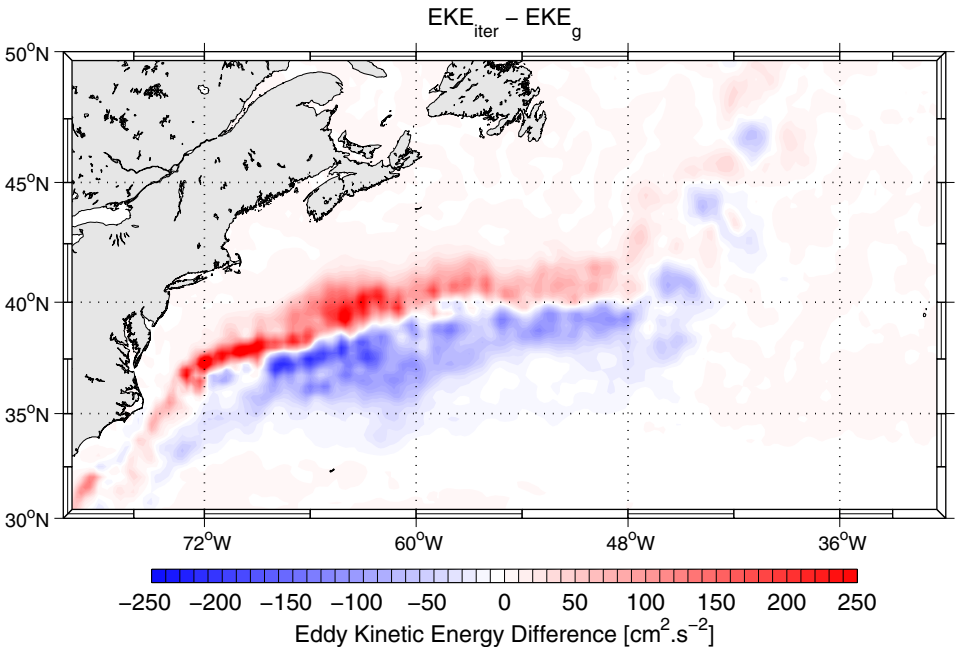

Figure 9. EKE difference ($cm^2\ s^{-2}$) between the iterative method and geostrophy in the Gulf Stream region.

The Mozambique Channel rings dominating the ocean circulation in the Mozambique Channel, the increase in velocities in the anticyclones is probably not statistically compensated by the decrease in the cyclones. This signature is clearly visible in EKE computed from AVISO altimetry from October 1992 to July 2012 using the different methods (Figure 8). Although geostrophic EKE shows values among the highest in the world ocean, reaching 1400 $cm^2\ s^{-2}$ in the central Mozambique Channel (Figure 8a), addition of inertia results in an EKE attaining 1800 $cm^2\ s^{-2}$ in the same region (Figure 8b). Differences of 300–500 $cm^2\ s^{-2}$ follow the track of the Mozambique Channel rings along the western side of the Mozambique Channel [*Halo et al*., 2014] (Figure 8c).

A secondary source of eddy variability south of Madagascar is known to favor the generation of dipoles, the cyclones being at the northern side of the anticyclones [*de Ruijter et al*., 2004]. Because of this asymmetry, the integration of inertia results in a diminution of EKE by 50 $cm^2\ s^{-2}$ in the southern tip of Madagascar and an increase of the same value further south (Figure 8c).

4. Discussion

It is well known that inertial effects are of importance in western boundary currents [*Charney*, 1955]. Indeed, direct ocean current observations have shown that the introduction of the centrifugal acceleration results in substantial differences in the estimate of sea level anomalies across Gulf Stream meanders [*Liu and Rossby*, 1993]. Similarly, comparison between velocities derived from drifting buoy trajectories and from altimetry in the Kuroshio is improved when the centrifugal acceleration is taken into account [*Uchida et al*., 1998]. These effects appear even more spectacular in the energetic coherent structures present in the region of western boundary currents, such as the Mozambique Channel rings.

Here we propose three simple methods to include the contribution of the inertial effects when deriving ocean current velocities from altimeter SSH. This additional physics easily improve the solution without the introduction of tunable parameters. As a result, they can be immediately applied for any ocean basin. Using these methods, we can infer a figure equivalent to the difference between drifting buoy EKE and altimetry geostrophic EKE shown by *Fratantoni* [2001] for the Gulf Stream region. Figure 9, presenting the difference between EKE from the iterative method and EKE from geostrophy, provides a quantification and confirms the hypothesis of *Maximenko and Niiler* [2006] that centrifugal accelerations should be the main cause of the difference reported by *Fratantoni* [2001].

Operational surface ocean currents are produced by adding an Ekman component to altimetry derived geostrophic currents [*Lagerloef et al*., 1999; *Sudre et al*., 2013]. The frictional parameters used for the Ekman component are in general statistically derived from the currents obtained from surface drifters [*Sudre et al*., 2013]. This is obtained by subtracting the geostrophic part to the drifters movement. In the context of large inertia, a net improvement of this residual should be obtained by using our proposed methodology to derive the non-Ekman velocities.

5. Conclusion

We have shown here that the effects related to inertia, and particularly the centrifugal acceleration, are significant when deriving velocities around eddies in the Mozambique Channel. This should explain the bias observed when comparing geostrophic velocities from altimetry with direct in situ measurements in the Mozambique Channel [*Ternon et al*., 2014]. Errors up to 50 cm s^{-1} could be accounted for the omission of these accelerations.

We have proposed three simple methods to incorporate inertia when deriving ocean velocities from AVISO-gridded altimetry. The iterative method, although more numerically expensive, gives the most satisfactory approximation of the surface currents in comparison to the other methods. When computing velocities in the central Mozambique Channel, the addition of inertia leads to a reduction of the errors by at least a factor of 3 in comparison to geostrophy. This could have important implications for operational products of surface ocean currents, as well as for the quantification of relative dispersion processes associated with eddy/eddy interactions which could influence marine life [*Tew-Kai et al*., 2009].

Since they are not associated with statistically defined/tunable parameters, these methods could easily be applied at global scale. Note that since current AVISO altimetry does not resolve small-scale structures, errors should still be large for the smaller eddies. Although inertia is already significant for AVISO altimetry gridded at 1/4° resolution, it would be much more critical when higher-resolution altimetry will be available with the Surface Water and Ocean Topography (SWOT) mission.

Acknowledgments
The altimeter products were produced by Ssalto/Duacs and distributed by Aviso, with support from Cnes (http://www.aviso.oceanobs.com/duacs/). Published with the support of AIRD.

References

Arnason, G., G. J. Haltiner, and M. J. Frawley (1962), Higher order geostrophic wind approximations, *Mon. Weather Rev.*, *90*, 175–185.
Backeberg, B. C., P. Penven, and M. Rouault (2012), Impact of intensified Indian Ocean winds on the mesoscale variability of the Agulhas system, *Nat. Clim. Change*, *2*, 608–612.
Bakun, A. (2006), Fronts and eddies as key structures in the habitat of marine fish larvae: Opportunity, adaptive response and competitive advantage, *Sci. Mar.*, *70*, 105–122.
Callen, J. D. (2003), *Fundamentals of Plasma Physics*, Univ. of Wis., Madison.
Charney, J. G. (1955), The Gulf Stream as an inertial boundary layer, *Proc. Natl. Acad. Sci. U. S. A.*, *41*, 731–740.
de Ruijter, W. P. M., H. Ridderinkhof, J. R. E. Lutjeharms, M. W. Schouten, and C. Veth (2002), Observations of the flow in the Mozambique Channel, *Geophys. Res. Lett.*, *29*(10), 140–1–140-3, doi:10.1029/2001GL013714.
de Ruijter, W. P. M., H. M. van Aken, E. J. Beier, J. R. E. Lutjeharms, R. P. Matano, and M. W. Schouten (2004), Eddies and dipoles around South Madagascar: Formation, pathways and large-scale impact, *Deep Sea Res., Part I*, *51*, 383–400.
Ducet, N., P. Y. Le Traon, and G. Reverdin (2000), Global high-resolution mapping of ocean circulation from TOPEX/Poseidon and ERS-1 and −2, *J. Geophys. Res.*, *105*, 19,477–19,498.
Endlich, R. (1961), Computation and uses of gradient winds, *Mon. Weather Rev.*, *89*, 187–191.
Fratantoni, D. M. (2001), North Atlantic surface circulation during the 1990's observed with satellite-tracked drifters, *J. Geophys. Res.*, *106*, 22,067–22,093.
Gold, E. (1908), The relation between wind velocity at one thousand meters altitude and the surface pressure distribution, *Proc. R. Soc. London, Ser. A*, *80*, 436–443.
Gründlingh, M. L. (1995), Tracking eddies in the southeast Atlantic and southwest Indian Oceans with TOPEX/Poseidon, *J. Geophys. Res.*, *100*, 24,977–24,986.
Halo, I. (2012), The Mozambique Channel eddies: Characteristics and mechanisms of formation, Ph.D. thesis, Univ. of Cape Town, Cape Town, South Africa.
Halo, I., B. Backeberg, P. Penven, I. Ansorge, C. Reason, and J. Ullgren (2014), Eddy properties in the Mozambique Channel: A comparison between observations and two numerical ocean circulation models, *Deep Sea Res., Part II*, doi:10.1016/j.dsr2.2013.10.015, in press.
Holton, J. R. (1992), *An Introduction to Dynamic Meteorology*, 3rd ed., 511 pp., Academic, San Diego, Calif.
Knox, J. A., and P. R. Ohmann (2006), Iterative solutions of the gradient wind equation, *Comput. Geosci.*, *32*, 656–662.
Lagerloef, G. S. E., G. T. Mitchum, R. B. Lukas, and P. P. Niiler (1999), Tropical Pacific near-surface currents estimated from altimeter, wind, and drifter data, *J. Geophys. Res.*, *104*, 23,313–23,326.
Liu, M., and T. Rossby (1993), Observations of the velocity and vorticity structure of Gulf Stream meanders, *J. Phys. Oceanogr.*, *23*, 329–345.
Maximenko, N., and P. Niiler (2006), Mean surface circulation of the global ocean inferred from satellite altimeter and drifter data, in *Proceeding of Symposium on 15 years of Progress in Radar Altimetry*, p. 614, Eur. Space Agency Spec. Publ., ESA Publications Division, Noordwijk, Netherlands.

Picaut, J., S. P. Hayes, and M. J. McPhaden (1989), Use of the geostrophic approximation to estimate time-varying zonal currents at the Equator, *J. Geophys. Res.*, *94*, 3228–3236.

Quartly, G. D., and M. A. Srokosz (2003), A visible record of eddies in the southern Mozambique Channel, in *Proceedings IEEE International on Geoscience and Remote Sensing Symposium, 2003, IGARSS '03*, vol. 2, pp. 957–959, IEEE Computer Society, Los Alamitos, Calif.

Rio, M.-H., S. Guinehut, and G. Larnicol (2011), New CNES-CLS09 global mean dynamic topography computed from the combination of GRACE data, altimetry, and in situ measurements, *J. Geophys. Res.*, *116*, C07018, doi:10.1029/2010JCOO6505.

Schouten, M. W., W. P. M. de Ruijter, P. J. van Leeuwen, and H. Ridderinkhof (2003), Eddies and variability in the Mozambique Channel, *Deep Sea Res., Part II*, *50*(12–13), 1987–2003.

Sudre, J., C. Maes, and V. Garcon (2013), On the global estimates of geostrophic and Ekman surface currents, *Limnol. Oceanogr. Methods*, *3*, 1–20.

Swart, N. C., J. R. E. Lutjeharms, H. Ridderinkhof, and W. P. M. de Ruijter (2010), Observed characteristics of Mozambique Channel eddies, *J. Geophys. Res.*, *115*, C09006, doi:10.1029/2009JC005875.

Ternon, J. F., M. J. Roberts, T. Morris, L. Hancke, and B. Backeberg (2014), In situ measured current structures of the eddy field in the Mozambique Channel, *Deep Sea Res., Part II*, doi:10.1016/j.dsr2.2013.10.013, in press.

Tew-Kai, E., V. Rossi, J. Sudre, H. Weimerskirch, C. Lopez, E. Hernandez-Garcia, F. Marsac, and V. Garon (2009), Top marine predators track Lagrangian coherent structures, *Proc. Natl. Acad. Sci. U. S. A.*, *106*, 8245–8250.

Uchida, H., S. Imawaki, and J.-H. Hu (1998), Comparison of Kuroshio surface velocities derived from satellite altimeter and drifting buoy data, *J. Oceanogr.*, *54*, 115–122.

Weimerskirch, H., M. Le-Corre, S. Jaquemet, and M. P. F. Marsac (2004), Foraging strategy of a top predator in tropical waters: Great frigatebirds in the Mozambique Channel, *Mar. Ecol. Prog. Ser.*, *275*, 297–308.